Interaction cross sections for light neutron-rich nuclei

B. A. Brown and S. Typel
Department of Physics and Astronomy and National Superconducting Cyclotron Laboratory, Michigan State University, East Lansing, Michigan 48824-1321

W. A. Richter
Department of Physics, University of Stellenbosch, Stellenbosch 7600, South Africa
(Received 13 July 2001; published 20 December 2001)

Interaction cross sections for nuclei with $Z=2-12$ on a ^{12}C target are calculated in the Glauber model with matter densities obtained from Skyrme Hartree-Fock and relativistic Dirac potentials. The shell-model orbital occupations and separation energies are taken from configuration-mixing calculations and experimental spectroscopic data. Halo effects are present in the most neutron-rich C and N isotopes. The rms matter radii and interaction cross section exhibit a kink at $N=14$ which can be associated with a change in the mean-field potential when the $1s_{1/2}$ orbit is being filled.

DOI: 10.1103/PhysRevC.65.014612 PACS number(s): 24.10.−i, 21.60.−n, 25.60.Dz, 25.70.Gh

The interaction cross sections of high-energy light radioactive beams provided one of the first clear indications for the existence of neutron halo phenomena [1]. Recent high-energy cross section data for $Z=6-9$ [2] together with other data [3–5] now provide a wider experimental picture for the interpretation of neutron halos and skins in light nuclei. One of the first microscopic theoretical interpretations for the cross section data was given by the Glauber reaction model with matter densities obtained from the Hartree-Fock (HF) model [6]. In this paper we present an updated Glauber model interpretation of the interaction cross sections for $Z=2-12$ based upon densities obtained in mean-field models. The overall comparison with experiment is excellent, and some new features emerge from the calculations.

The matter densities were calculated in a spherical HF basis with the SKX Skyrme interaction [7], although the general features we discuss here emerge from all Skyrme interactions [8]. We also comment on the results with a relativistic Dirac-Hartree model. The reaction model is the zero-range Glauber model described in Ref. [6]. The input to the Glauber model is an *NN* interaction with effective cross sections [9] of 40.0 mb for 680–740 MeV/nucleon, 40.9 mb for 790 MeV/nucleon, and 44.0 mb for 950–1020 MeV/nucleon. The experimental data for the cross sections on ^{12}C were taken from the compilation of Ozawa *et al.* [10] (the beam energies were 790–800 MeV/nucleon for $Z=2-5$ and 950–1020 MeV/nucleon for $Z=6-12$, with the exceptions of ^{10,11}B data taken at 950–960 MeV/nucleon, and ^{9,10,11,15}C, ^{12,13,17}N, ^{13,14,15}O, ^{17}F, and ^{17}Ne data taken at 670–740 MeV/nucleon.)

The HF calculations start with a sequential filling of the orbits in the order $0s_{1/2}$, $0p_{3/2}$, $0p_{1/2}$, $0d_{5/2}$, $1s_{1/2}$, and $0d_{3/2}$. This is accurate enough for well-bound nuclei near stability. The single-particle energies from SKX agree with experiment to within 1–2 MeV [7]. As discussed in Ref. [6], when one approaches the neutron drip line the matter radii are sensitive to the separation energies, especially for the low-l orbits. The separation energy also depends upon the pairing and collective aspects of the residual interaction which are not present in the HF mean field. Thus for the nuclei near the drip line we constrain orbit occupations and separation energies in the HF by the results of shell-model configuration mixing calculations and experimental data on binding energies and spectroscopic factors. The HF potentials are obtained from the spherical densities for protons ($t_z=-1/2$) and neutrons ($t_z=1/2$):

$$\rho(r,t_z)=\sum_{n,l,j} n_{n,l,j,t_z}\,\rho(r)_{n,l,j,t_z}, \tag{1}$$

where n_{n,l,j,t_z} are the occupation numbers and $\rho(r)_{n,l,j,t_z}$ are the spherical single-particle densities for each orbital. The sum runs over the filled core orbits and the partially filled valence orbits, and the normalizations are $\Sigma_{n,l,j} n_{n,l,j,t_z}=Z/N$ for protons and neutrons, respectively. For the valence orbits we obtain the orbital occupations from the experimental knockout reactions and from shell-model configuration mixing calculations discussed below.

The separation energy constraint was made by multiplying the central HF potential for a given orbital by a factor such that the single-particle energy for that orbital is equal to its observed separation energy. This adjustment is partly to compensate for the residual interactions beyond mean field such as pairing and deformation, which are not present in the spherical calculations. In addition, the Skyrme parameters are based upon global fits to nuclear properties, and the mean-field binding energies are usually not calculated to better than a few MeV. Thus near the drip line where the asymptotics in the densities are sensitive to changes in the separation energies on the order of 100 keV, the mean-field calculations are very inadequate unless some separation energy constraint is made. For example, for the $1/2^+$ ground state of ^{11}Be deformation and pairing lead to about a 5 MeV increase in its binding compared to the spherical mean field [11]. The spherical mean-field potential for the $1s_{1/2}$ orbit must be increased by about 20% in order to compensate for this increased binding and give the observed separation energy of 0.5 MeV. However, for neutron-rich nuclei with $Z\geqslant 8$, no modifications to the HF potential were required,

TABLE I. Constraints on the neutron occupation numbers and separation energies.

Nucleus	Core	Valence orbit	Occupation	Separation energy (MeV)
^{11}Li	^{9}Li	$1s_{1/2}$	1.0	0.3
		$0p_{1/2}$	1.0	0.3
^{11}Be	^{10}Be	$1s_{1/2}$	0.75	0.5
		$0d_{5/2}$	0.25	3.8
^{12}Be	^{10}Be	$1s_{1/2}$	0.67	3.2
		$0d_{5/2}$	0.67	4.5
		$1p_{1/2}$	0.67	3.4
^{14}Be	^{12}Be	$1s_{1/2}$	1.0	1.3
		$0d_{5/2}$	1.0	1.3
^{14}B	^{13}B	$1s_{1/2}$	0.66	0.9
		$0d_{5/2}$	0.34	0.9
^{15}B	^{13}B	$1s_{1/2}$	1.0	2.7
		$0d_{5/2}$	1.0	2.7
^{17}B	^{13}B	$1s_{1/2}$	1.5	1.4
		$0d_{5/2}$	2.5	1.4
^{19}B	^{13}B	$1s_{1/2}$	2.0	1.0
		$0d_{5/2}$	4.0	1.0
^{15}C	^{14}C	$1s_{1/2}$	1.00	1.2
^{16}C	^{14}C	$1s_{1/2}$	0.60	4.2
		$0d_{5/2}$	1.40	4.9
^{17}C	^{14}C	$1s_{1/2}$	0.40	3.2
		$0d_{5/2}$	2.60	3.2
^{19}C	^{14}C	$1s_{1/2}$	0.60	0.6
		$0d_{5/2}$	4.40	2.6
^{22}N	^{21}N	$1s_{1/2}$	1.0	1.2
^{23}O	^{22}O	$1s_{1/2}$	1.0	2.7
^{24}F	^{23}F	$1s_{1/2}$	1.0	3.8

since the separation energies are not extremely small, and because the values obtained with SKX are within about 1 MeV of the experimental values. Also for nuclei near stability, separation-energy constraints are not required—the separation energies are large enough so that the cross-section results obtained with and without separation energy constraints are essentially the same.

The occupation-number and separation-energy constraints are summarized in Table I. For nuclei where there are narrow final states available for one-neutron removal, we use the one-neutron separation energies associated with the particular nlj value. Of the cases in Table I, ^{17}C is rather unusual because the removal of a neutron leads primarily to the excited 2^+ state of ^{16}C [12] (not to the ground state). For the two cases of ^{11}Li and ^{14}Be which have no sharp intermediate states we use the two-neutron separation energy for all nlj values. The separation energies are based on the Audi-Wapstra mass table [13]. An exception is the one-neutron separation energy of ^{19}C which is taken as 0.6 MeV from the analysis of Ref. [12]. The Audi-Wapstra one-neutron separation energy for ^{19}B is based on their extrapolations and has a larger error, so the calculation for ^{19}B is not very reliable, unless the extrapolated value is confirmed by experiment.

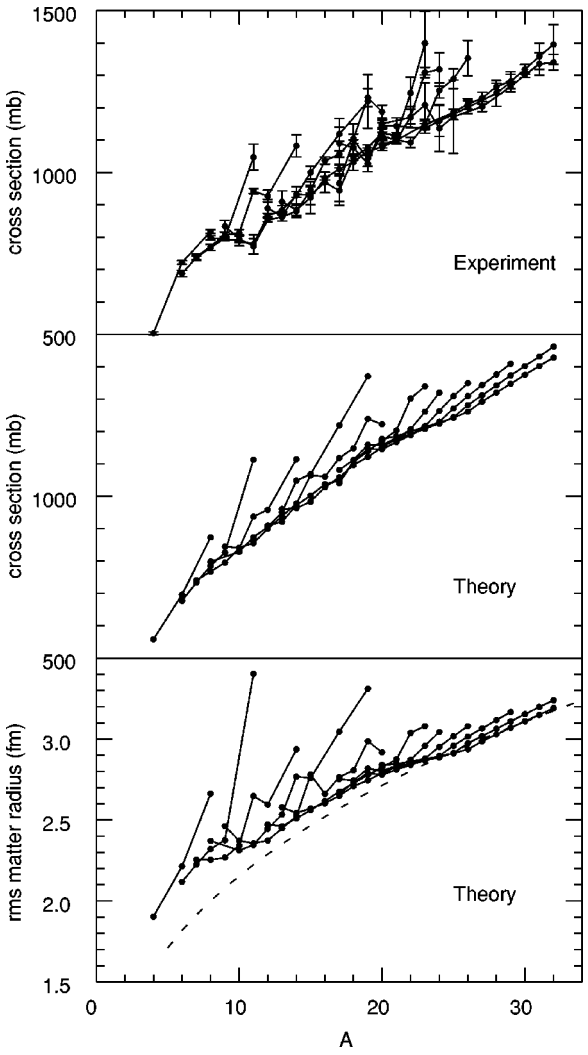

FIG. 1. Matter rms radii and interaction cross sections vs nucleon number A. Bottom: calculated matter radii. Middle: calculated interaction cross sections. Top: experimental interaction cross sections. The dashed line in the bottom panel is $A^{1/3}$.

The occupations given in Table I are those obtained from the WBT interaction [14] in the p-sd basis, except those for ^{11}Li and ^{12}Be as discussed below. For $Z \geqslant 8$ the WBT results are equivalent to those for the sd shell with the USD interaction [15]. The small occupation of the $0d_{3/2}$ orbit is added to that of the $0d_{5/2}$ orbit. For many cases the calculated spectroscopic factors can be compared to those obtained from recent one-neutron knockout reactions. The spectroscopic results for the carbon isotopes [12,16], ^{14}B [17], and ^{11}Be [18] are consistent with those obtained from WBT. The knock-out experiment on ^{12}Be [19] has been interpreted in terms of mixed $0\hbar\omega$ and $2\hbar\omega$ configurations with the resulting occupations given in Table I. The ^{11}Li occupations are taken from Ref. [20].

The calculated rms matter radii and interaction cross sections for $Z=2-12$ are shown in Fig. 1 as a function of nucleon number A and in Fig. 2 as a function of neutron number N. The various isotopic chains are connected by lines. The purpose of these figures is to show the overall A

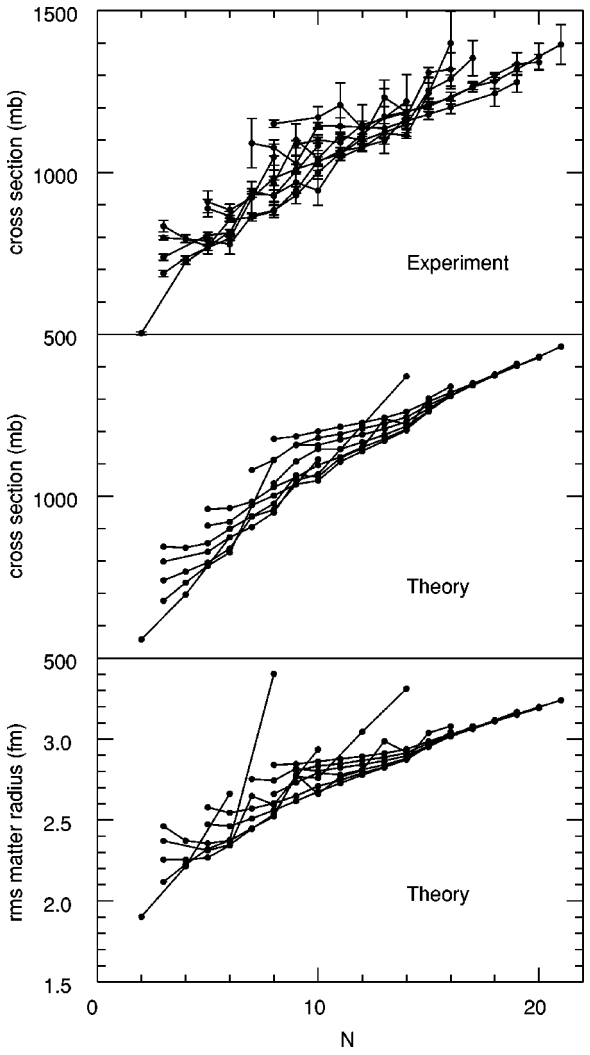

FIG. 2. Matter rms radii and interaction cross sections vs neutron number *N*. Bottom: calculated matter radii. Middle: calculated interaction cross sections. Top: experimental interaction cross sections.

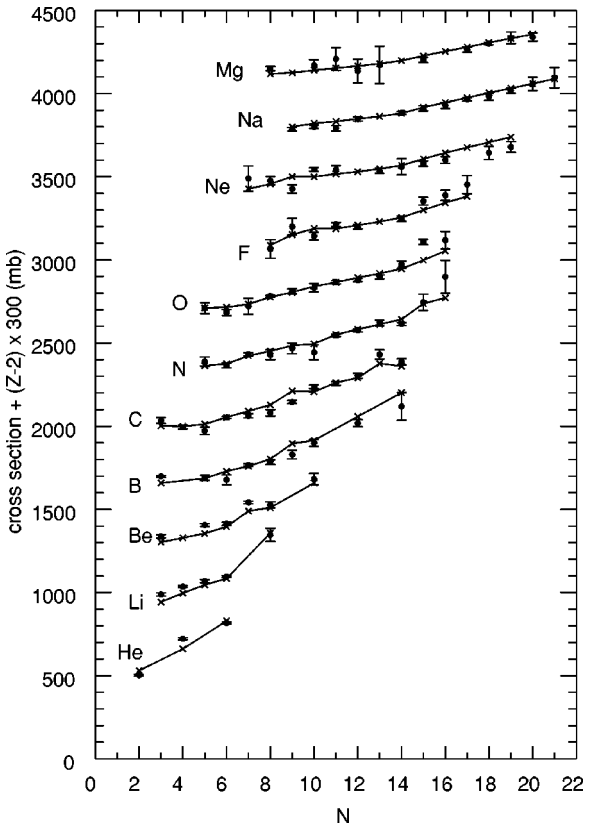

FIG. 3. Calculated and experimental interaction cross sections. The values for Z are separated by the addition of $300(Z-2)$.

and N dependence. Detailed comparisons for each Z value are made in Fig. 3. There are several interesting trends. Below $A=20$ the radii and cross sections lie in a narrow band above which lie a few points related to the halo nuclei ^{11}Li, ^{11}Be, ^{14}Be, ^{17}B, ^{19}B, and ^{19}C. Beyond $A=20$ there is an upward bend in the theoretical curves which is partly reflected in the data (see Fig. 3 for a detailed comparison with each Z value). In Fig. 2 the upward bend is seen to be associated with a kink at $N=14$.

The interaction cross sections are compared with experiment in Fig. 3. In this figure we add $300(Z-2)$ to experiment and theory in order to display the data for the various Z values in one figure. All of the calculated cross sections are multiplied by 0.95 to obtain an optimum overall agreement with experiment. The agreement with experiment is impressive, even for the halo nuclei ^{11}Li, ^{11}Be, ^{14}Be, ^{17}B, ^{19}B, and ^{19}C. It has been shown that correlation effects in the nuclear wave functions which go beyond the simple folding of the spherical target and projectile densities are important for the cross sections in halo nuclei [21–23]. Without these correlations, the calculated cross sections for the two-neutron halo nuclei, ^{6}He, ^{11}Li, and ^{14}Be are about 10% larger than experiment [21]. It has also been pointed out that nuclear correlations also should reduce the interaction cross sections for normal (nonhalo) nuclei [24]. Thus our empirical reduction factor of 0.95 may be attributed to an average of the nuclear correlation effects for normal and halo nuclei.

There are a few details which do not agree within experimental error. One of these is the enhancement in the calculated ^{15}C and ^{14}B ($N=9$) cross sections which does not show up in the experiment trend. The theoretical enhancement is due to the relatively loose binding of the $1s_{1/2}$ orbit (see Table I). Another is the relatively large experimental cross section for ^{23}O ($N=15$) compared to theory. Overall, the data supports the halo nature for some nuclei, as well as the upward bend at $N=14$.

The kink at $N=14$ is related to a change in the self-consistent potential. Between $N=8$ and $N=14$ the $0d_{5/2}$ orbit is mainly being filled and the neutron density increases at the nuclear surface. Beyond $N=14$ neutrons start to occupy the $1s_{1/2}$ orbit which gives an additional interior contribution to the density on top of that already present from the filled $0s$ and $0p$ orbits. The matter densities for the even-even oxygen isotopes from $N=10$ to $N=16$ are shown in Fig. 4. The surface density gradually increases as a function of neutron number and the resulting HF potential for neutrons monotonically increases in radius as a function of neutron number.

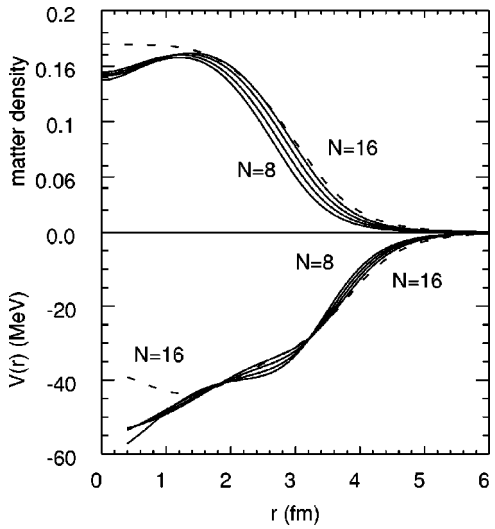

FIG. 4. The SKX HF matter densities and neutron potentials for ^{16,18,20,22,24}O corresponding to $N=8,10,12,14$ (solid lines) and 16 (dashed line).

There is a discontinuous change in the potential when neutrons are added to the $1s_{1/2}$ orbit such that the potential becomes suddenly weaker in the interior and hence pushes out the neutron density, especially for the $1s_{1/2}$ orbit itself.

We can quantitatively define the kink by the ratio

$$k=\frac{\sigma(N=16)-\sigma(N=14)}{\sigma(N=14)-\sigma(N=12)}\approx\frac{\langle r_m^2\rangle(N=16)-\langle r_m^2\rangle(N=14)}{\langle r_m^2\rangle(N=14)-\langle r_m^2\rangle(N=12)}, \tag{2}$$

where $\langle r_m^2\rangle$ is the mean-square matter radius and σ is the interaction cross section. The approximate equality between the value obtained from the mean-square matter radius and the interaction cross section follows numerically from the calculations as well as from the usual approximate geometric relationship [1] between the interaction cross section and the rms matter radii of the target $R_t=\sqrt{\langle r_m^2\rangle_t}$ and the projectile $R_p=\sqrt{\langle r_m^2\rangle_p}$, given by $\sigma=\pi(R_t+R_p)^2$.

The k value will have some Z dependence, and we will discuss below the numerical results for the oxygen isotopes ($Z=8$). For the oxygen isotopes there is a strong shell gap at $N=14$ and $N=16$ in both experiment and theory [25]. The occupation of the $1s_{1/2}$ neutron orbit increases rapidly from 0.26 in ^{22}O ($N=14$) to 1.91 in ^{24}O ($N=16$). For higher Z values the $1s_{1/2}$-$0d_{3/2}$ gap is gradually washed out by the proton-neutron interaction [26]. For example, for $Z=12$ the $1s_{1/2}$ occupancy increases from 0.56 in ^{26}Mg ($N=14$) to 1.12 in ^{28}Mg ($N=16$).

The SKX HF interaction gives $k=2.0$ for the oxygen isotopes. We have investigated a variety of other Skyrme interactions and find that they all give values of k between 1.9 and 2.1 as long as the single-particle energy of the $1s_{1/2}$ orbit is within about 1 MeV of the experimental separation energy. The Woods-Saxon potential gives $k\approx1.5$ which is a measure of the small skin or halo effect associated with the $1s_{1/2}$ orbit. Since the Woods-Saxon potential changes smoothly as a function of N, there is no special change in the potential when the $1s_{1/2}$ orbit is being filled. We have also investigated the NL3 [27] and VDD [28] relativistic Hartree models for the oxygen isotopes and find $k=2.3$ for NL3 and $k=2.6$ for VDD. So there is some model dependence in the kink value. The experimental cross section data for nitrogen, oxygen and fluorine would favor a kink value somewhat larger than the Skyrme result, whereas the data for $Z\geqslant10$ appear to have a smaller kink than in the calculation. But as a whole the data for $Z=7-12$ agree well with the Skyrme calculations.

In summary, we have shown that the complete set of interaction cross section data can be described by the Glauber model with matter densities obtained from mean-field models supplemented by constraints on the orbit occupations and separation energies of the most loosely bound valence orbits. A jump in the matter radii and interaction cross sections associated with a change in the mean-field potential when the $1s_{1/2}$ orbit is filled beyond $N=14$ in neutron-rich nuclei was discussed.

We acknowledge National Science Foundation Grant No. PHY-007091 and the South African National Research Foundation. We thank Jeff Tostevin for helpful comments on the paper.

[1] I. Tanihata *et al.*, Phys. Rev. Lett. **55**, 2676 (1985).
[2] A. Ozawa *et al.*, Nucl. Phys. **A691**, 599 (2001).
[3] T. Suzuki *et al.*, Phys. Rev. Lett. **75**, 3241 (1995).
[4] I. Tanihata *et al.*, Phys. Lett. **160B**, 380 (1985).
[5] I. Tanihata *et al.*, Phys. Lett. B **206**, 592 (1988).
[6] G.F. Bertsch, B.A. Brown, and H. Sagawa, Phys. Rev. C **39**, 1154 (1989).
[7] B.A. Brown, Phys. Rev. C **58**, 220 (1998).
[8] B.A. Brown and W.A. Richter, Phys. Rev. C **54**, 673 (1996).
[9] S.K. Charagi and S.K. Gupta, Phys. Rev. C **41**, 1610 (1990).
[10] A. Ozawa, T. Suzuki, and I. Tanihata (unpublished).
[11] H. Sagawa, B.A. Brown, and H. Esbensen, Phys. Lett. B **309**, 1 (1993).
[12] V. Maddalena *et al.*, Phys. Rev. C **63**, 024613 (2001).
[13] G. Audi and A.H. Wapstra, Nucl. Phys. **A595**, 409 (1995).
[14] E.K. Warburton and B.A. Brown, Phys. Rev. C **46**, 923 (1992).
[15] B.A. Brown and B.H. Wildenthal, Annu. Rev. Nucl. Part. Sci. **38**, 29 (1988).
[16] D. Bazin *et al.*, Phys. Rev. C **57**, 2156 (1998).
[17] V. Guimaraes *et al.*, Phys. Rev. C **61**, 064609 (2000).
[18] T. Aumann *et al.*, Phys. Rev. Lett. **84**, 35 (2000).
[19] A. Navin *et al.*, Phys. Rev. Lett. **85**, 266 (2000).
[20] H. Simon *et al.*, Phys. Rev. Lett. **83**, 496 (1999).
[21] J.S. Al-Khalili, I.J. Thompson, and J.A. Tostevin, Phys. Rev. Lett. **76**, 3903 (1996); Phys. Rev. C **54**, 1843 (1996).

[22] H. Esbensen and G.F. Bertsch, Phys. Rev. C **59**, 3240 (1999).
[23] R.C. Johnson and C.J. Goebel, Phys. Rev. C **62**, 027603 (2000), and references therein.
[24] H. Nishioka and R.C. Johnson, Phys. Rev. C **22**, 2457 (1980); J. Phys. G **8**, 39 (1982).
[25] P.G. Thirolf *et al.*, Phys. Lett. B **485**, 16 (2000).
[26] T. Otsuka, R. Fujimoto, Y. Utsuno, B.A. Brown, M. Honma, and T. Mizusaki, Phys. Rev. Lett. **87**, 082502 (2001).
[27] G.A. Lalazissis, J. König, and P. Ring, Phys. Rev. C **55**, 540 (1997).
[28] S. Typel and H.H. Wolter, Nucl. Phys. **A656**, 331 (1999)